Electron-electron interaction effect on longitudinal and Hall transport in thin and thick $Ag_x(SnO_2)_{1-x}$ granular metals

Ya-Nan Wu, Yan-Fang Wei, and Zhi-Qing Li*
Tianjin Key Laboratory of Low Dimensional Materials Physics and Preparing Technology, Department of Physics, Tianjin University, Tianjin 300072, China

Juhn-Jong Lin†
NCTU-RIKEN Joint Research Laboratory, Institute of Physics and Department of Electrophysics, National Chiao Tung University, Hsinchu 30010, Taiwan

(Received 4 January 2015; revised manuscript received 13 February 2015; published 3 March 2015)

We study the temperature behaviors of the Hall coefficient, R_H, and longitudinal conductivity, σ, of two series of $Ag_x(SnO_2)_{1-x}$ (x being the Ag volume fraction) granular films lying in the metallic regime. The first (second) series of films are ~500 (~9) nm thick and constitute a three- (two-) dimensional granular array. In the high-x regime with $g_T \gg g_T^c$ (g_T being the dimensionless intergrain tunneling conductance, and g_T^c being the critical tunneling conductance at the percolation threshold), we observe a $R_H \propto \ln T$ law from ~6 to 300 K. This $\ln T$ behavior is independent of array dimensionality. We also observe a $\sigma \propto \ln T$ law in the temperature range ~20–100 K. Below ~10 K, the temperature behavior of σ changes to a $\sqrt{T}$ dependence in thick films, while it changes to a different $\ln T$ dependence in thin films. The overall R_H and σ characteristics can be explained by the electron-electron interaction (EEI) effects in the presence of granularity. As x is reduced and approaches the percolation threshold, we found that the $\ln T$ dependences of R_H and σ still hold for a wide temperature range. We propose an explanation for the long-standing puzzle of the $\sigma \propto \ln T$ dependence, which has previously been frequently observed in composite systems near the quantum percolation threshold, as arising from the same EEI effect considered in the recent theory of granular metals.

DOI: 10.1103/PhysRevB.91.104201 PACS number(s): 73.63.−b, 72.20.My, 72.80.Tm

I. INTRODUCTION

Granular metals are composite materials consisting of immiscible metals and insulators. The electronic conduction properties of granular films have attracted much interest in past decades, and good progress has been made in this area of research [1–11]. For example, theories on the electrical conduction processes in the metallic, dielectric, and metal-insulator transition regimes have been formulated [1,2]. The influence of intergrain coupling on the ground-state properties of insulator-superconductor systems has been addressed [3,5]. The local quantum-interference effect on the Hall transport properties near the quantum percolation threshold has also been put forward [6–8]. Nevertheless, the electron-electron interaction (EEI) effect on the charge transport properties of "granular metals" remains a challenging and complex problem. It was only recently that theoretical studies found that the EEI effect on the transport properties *in the presence of granularity* is distinct from that of "homogeneous disordered metals" [3,4,12–15]. Here a granular metal means a metal-dielectric composite lying above the percolation threshold.

The recent theory of granular metals is concerned with the strong intergrain coupling limit of $g_0 \gg g_T \gg 1$, where the dimensionless conductance of a metal grain $g_0 = G_0/(2e^2/\hbar)$ (G_0 being the conductance of a metal grain), the dimensionless intergrain tunneling conductance $g_T \equiv G_T/(2e^2/\hbar)$ (G_T being the intergrain tunneling conductance), e is the electronic charge, and $\hbar$ is the Planck constant divided by 2π. The theory explicitly predicts, due to the EEI effect in the presence of granularity, logarithmic temperature corrections to both longitudinal conductivity, σ, and Hall coefficient, R_H. Moreover, the theory predicts that the $\ln T$ dependences of σ and R_H are independent of the granular array dimensionality. The underlying physical origin of the $\sigma \propto \ln T$ behavior is subtly different from that of the $R_H \propto \ln T$ behavior. The former arises from the renormalization of intergrain tunneling conductance g_T [3,13], while the latter stems from the virtual electron diffusion inside individual grains [4].

Soon after the theoretical finding of the $\ln T$ corrections, the conductivities of several granular systems were measured, including Pt/C composite nanowires [16,17], B-doped nanocrystalline diamond films [18], and granular Cr films [19]. The $\sigma \propto \ln T$ law was confirmed. However, the $\ln T$ correction to R_H has rarely been experimentally tested, owing to the difficulty in measuring this physical quantity in the metallic regime. Indeed, the $R_H \propto \ln T$ law has only recently been observed by Zhang *et al.* [20] in a series of two-dimensional (2D) indium tin oxide (ITO) thin granular films, in which the carrier concentration is nearly three orders of magnitude lower than that in a typical metal. Because the theory predicts that the $R_H \propto \ln T$ law should hold regardless of the array dimensionality, it is of prime interest to test this prediction.

The theoretical calculations for the electronic conduction properties of granular metals can only obtain analytical results for σ and R_H in the strong coupling limit $g_T \gg 1$ [3,4,12–15,21]. However, it is empirically known that the EEI effect is enhanced with progressive decrease in g_T [3]. It is then desirable to explore how the EEI effect might affect the transport properties of samples with low g_T values. In this work, in addition to the strong coupling regime, we investigate the

*Electronic address: zhiqingli@tju.edu.cn
†Electronic address: jjlin@mail.nctu.edu.tw

narrow regime ($1 > g_T > g_T^c$) near the percolation threshold, where g_T^c is the critical tunneling conductance associated with the percolation threshold. In our samples used in this work, $g_T^{c,3D} \simeq 0.22$ and $g_T^{c,2D} \simeq 0.5$.

We study the EEI effect on the electrical transport properties of two series of $Ag_x(SnO_2)_{1-x}$ granular films prepared by the cosputtering method, where x denotes the Ag volume fraction. The first (second) series of films are ~500 (~9) nm thick and can be considered as three-dimensional (two-dimensional) arrays. There are several advantages for using this composite system. (1) Ag is a metal that possesses a high value of σ while a relatively low electron concentration, n, as compared with those in Cu, Al, Sn, Pb, Zn, and In [22]. A relatively low n facilitates the measurement of the temperature dependence of R_H. (2) Ag is immiscible with SnO_2 and can form stable spherical-shaped granules in the Ag-SnO_2 composite [23]. (3) The theoretical criterion $g_0 \gg g_T \gg 1$ for a composite system to possess sufficiently large intergrain tunneling and reveal global metallic features poses a stringent condition for experiments. We can carefully tune the individual sputtering powers in the Ag and SnO_2 targets to adjust the x (g_T) value of a given film and experimentally meet this criterion. We thus observe array dimensionality independent $R_H \propto \ln T$ and $\sigma \propto \ln T$ laws in both thin and thick films. (4) Moreover, the Ag-SnO_2 composite system allows us to study the low-x regime just above the percolation threshold, x_c. In this regime of $x \to x_c$ (corresponding to $g_T \to g_T^c$), we found that the $\ln T$ dependences of σ and R_H still prevail and can be seen in a wide T range. It should be remembered that this low-x regime lies outside the theoretical perturbation regime of $g_T \gg g_T^c$. Based on our results obtained in this narrow critical regime, we propose that the long-standing puzzle of the $\sigma \propto \ln T$ behavior previously observed by several groups in composite systems [24–33] near the percolation threshold is caused by the same EEI effect considered in the recent theory of granular metals [3,12–14].

The paper is organized as follows. In Sec. II, we describe our experimental method. In Sec. III we present our experimental results and theoretical analysis of the measured R_H and σ data based on the recent theory of granular metals. Our conclusion is given in Sec. IV.

II. EXPERIMENTAL METHOD

Our $Ag_x(SnO_2)_{1-x}$ granular films were deposited onto glass substrates held at room temperature by the cosputtering method. An Ag and a SnO_2 target, both with a diameter of 60 mm, were used as the sputtering sources. The details of the cosputtering deposition procedures were described previously [23]. Hall-bar-shaped samples (0.8 mm wide and 3.5 mm long) [8,20], defined by mechanical masks, were utilized for the measurements of R_H and σ between 2 and 300 K. The thicknesses of the films were measured with a surface profiler (Dektak, 6 M) for those films of ~500 nm thickness, and with a multipurpose diffractometer (X'pertPRO) by the low-angle x-ray diffraction method for those films of ~9 nm thickness. The Ag volume fraction x in each sample was obtained from the energy-dispersive x-ray spectroscopy analysis. The microstructures of the films were characterized by field emission transmission electron microscopy studies (TEM, Tecnai G2 F20). The electrical conductivity and Hall coefficient were measured using a physical property measurement system (PPMS-6000, Quantum Design), by employing the four-probe configuration. In the case of R_H measurements, in order to cancel out any unwanted misalignment voltages and thermomagnetic effect, a square-wave current operating at a frequency of 8.33 Hz was applied. The magnetic field was regulated to sweep from −2 to 2 T in steps of 0.2 T. In the case of σ measurements, a magnetic field of 7 T perpendicular to the film plane was applied to suppress the weak-localization effect [34–38]. More than eight samples for each series of films (~500 or ~9 nm thick) were measured. Table I lists the relevant parameters for only some representative samples.

III. RESULTS AND DISCUSSION

Figures 1(a) and 1(b) show the bright-field TEM images of the cross sections of two ~500 nm thick films with $x = 0.62$

TABLE I. Relevant parameters for selected 3D and 2D $Ag_x(SnO_2)_{1-x}$ granular films. t is the mean film thickness, x is Ag volume fraction, and c_d and n^* (g_T and σ_0) are adjustable parameters in Eq. (1) [Eq. (3)]. $g_T\tilde{\delta}/k_B$ ($= T^*$) is the characteristic crossover temperature defined in the text, and $\min(g_T E_c, E_{\rm Th})/k_B$ ($= T_{\rm max}^H$) is the upper bound temperature for Eq. (1) to hold. For samples with $g_T < 1$, these two characteristic temperatures were calculated by setting $g_T = 1$ (Ref. [13]). Note that in 2D, $\sigma_0 = \sigma_{\square,0}/t$, where $\sigma_{\square,0}$ is the classical sheet conductivity without the EEI effect.

t (nm)	x	ρ(300 K) ($\mu\Omega$ m)	c_d	n^* (10^{28} m^{-3})	g_T	σ_0 (S/m)	$g_T\tilde{\delta}/k_B$ (K)	$\min(g_T E_c, E_{\rm Th})/k_B$ (K)
508	0.64	4.0	1.3	3.6	12	249668	45 ± 38	2230 ± 637
573	0.62	5.2	1.6	1.8	9.5	193260	35 ± 29	1895 ± 542
493	0.60	7.5	1.1	2.6	4.4	132715	16 ± 14	879 ± 251
575	0.58	28.0	0.41	3.4	0.90	33069	3.6 ± 3.1	199 ± 57
545	0.56	37.6	0.54	3.8	0.58	23269	3.6 ± 3.1	199 ± 57
517	0.52	80.4	0.64	1.2	0.34	9377	3.6 ± 3.1	199 ± 57
8.9	0.72	9.3	1.7	2.8	9.1	109325	33 ± 28	1815 ± 516
8.6	0.70	23.0	1.3	2.9	3.2	44551	11 ± 9	633 ± 181
9.8	0.68	24.8	0.79	2.2	2.8	40974	10 ± 9	558 ± 160
8.9	0.67	29.8	0.95	2.2	2.5	34008	9.0 ± 8	495 ± 142
9.7	0.65	41.0	0.45	2.6	1.5	23751	5.5 ± 5	305 ± 87
8.4	0.64	61.6	0.63	2.2	1.0	15906	3.6 ± 3.1	199 ± 57

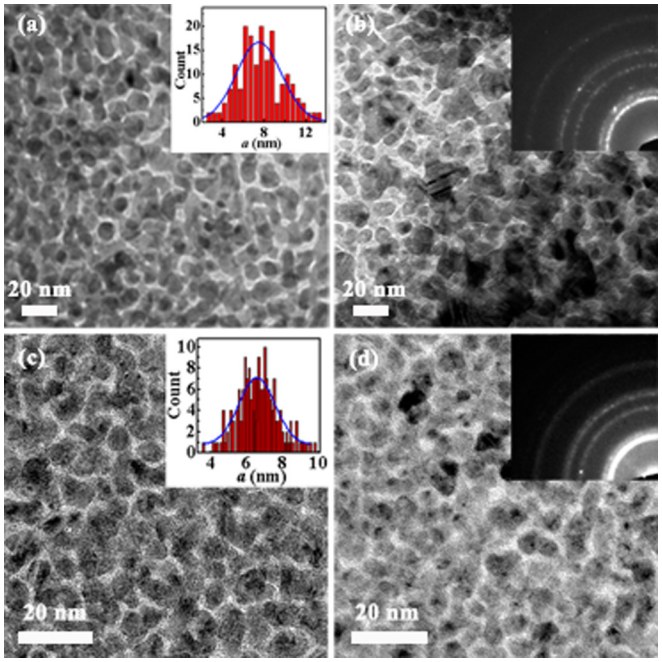

FIG. 1. (Color online) Bright-field cross-sectional TEM images for ~500 nm thick $Ag_x(SnO_2)_{1-x}$ films with $x \simeq$ (a) 0.62 and (b) 0.52, and top-view TEM images for ~9 nm thick films with $x \simeq$ (c) 0.70 and (d) 0.64. The insets in (a) and (c) show the corresponding grain size distribution histograms, and the insets in (b) and (d) show the respective selected-area electron-diffraction patterns.

and 0.52, respectively. The dark (bright) regions are Ag grains (SnO_2 matrix). We found that in films with $x \lesssim 0.65$ most of the Ag particles are relatively evenly dispersed in the SnO_2 matrix, while in films with $x \gtrsim 0.7$ most of the Ag particles are geometrically connected. The inset of Fig. 1(b) shows the selected-area electron-diffraction patterns. The bright diffraction rings arise from the patterns of face-centered cubic (fcc) Ag. No other diffraction patterns are found, indicating that SnO_2 forms an amorphous matrix while other AgSn alloy phases do not form in our films. The mean size (diameter), a, of Ag granules in films with $0.5 \lesssim x \lesssim 0.65$ is found to be 7 ± 2 nm, as evidenced in the inset of Fig. 1(a). Moreover, one sees in Figs. 1(a) and 1(b) that the Ag particles are approximately spherical in shape. A spherical structure was further confirmed by the top-view TEM images (not shown). The spherical-shaped characteristic of Ag particles, together with the aforementioned advantages, made Ag-SnO_2 granular films an ideal composite system for testing the recent theory of granular metals [3,4,12–15].

Figures 1(c) and 1(d) show the top-view TEM images of ~9 nm thick films with $x = 0.70$ and 0.64, respectively. One sees that this series of thin films also possesses typical granular characteristics, with Ag particles crystallizing in the fcc structure and SnO_2 forming an amorphous matrix. Again, the Ag particles are nearly spherically shaped, with a mean diameter $a \simeq 7 \pm 2$ nm in films with $0.64 \lesssim x \lesssim 0.72$. (In films with $x \gtrsim 0.74$, the Ag particles are geometrically connected.) In this case, each sample is only covered by one layer of Ag granules and forms a 2D random granular array. We reiterate that the ~500 thick films form 3D random granular arrays.

In our 3D films, the percolation threshold $x_c^{3D} \simeq 0.50$ was previously determined [23]. In this work, we focus on those films with $0.52 \lesssim x \lesssim 0.65$, in which the criterion $g_T \ll g_0$ is satisfied and the films reveal global metallic features. Similarly, we found in 2D films the percolation threshold $x_c^{2D} \simeq 0.63$. In this 2D case, we focus on those samples with $0.64 \lesssim x \lesssim 0.72$.

A. Logarithmic temperature dependence of Hall coefficient in the $g_T \gg g_T^c$ regime

We first consider the temperature behavior of R_H in the samples lying in the strong coupling regime of $g_T \gtrsim 5g_T^c$. This condition corresponds to $x \gtrsim 0.59$ in 3D films and $x \gtrsim 0.67$ in 2D films. Figures 2(a) and 2(b) show the variation of R_H with logarithm of temperature for two 3D films with x as indicated. Clearly, one observes a $R_H \propto \ln T$ law in a wide T range ~6–300 K. Theoretically, it has recently been formulated that the virtual electron diffusion inside individual grains causes a $\ln T$ correction to the Hall transport. The EEI correction to R_H in the temperature range $T^* \lesssim T \lesssim T_{\max}^H$, where the characteristic temperature $T^* = g_T\tilde{\delta}/k_B$ ($\tilde{\delta}$ being the mean energy level spacing in a grain, and k_B being the Boltzmann constant) and the upper bound temperature $T_{\max}^H \equiv \min(g_T E_c, E_{\rm Th})/k_B$, can be written as [4,15]

$$R_H = \frac{1}{n^* e}\left[1 + \frac{c_d}{4\pi g_T}\ln\left(\frac{\min(g_T E_c, E_{\rm Th})}{k_B T}\right)\right], \quad (1)$$

where n^* is the effective carrier concentration, c_d is a numerical lattice factor of order unity, $E_{\rm Th}$ is the Thouless energy, and E_c is the charging energy of an isolated metal grain. For a granular metal, one can write $\tilde{\delta} = 1/[N(E_F)V]$ [where $N(E_F)$ is the electronic density of states at the Fermi energy E_F, and V is the grain volume], $E_{\rm Th} = 4\hbar D/a^2$ (where D is the electron diffusion constant), and $E_c = e^2/(4\pi\epsilon_0\epsilon_r a)$ [where ϵ_0 (ϵ_r) is the permittivity of vacuum (dielectric matrix)] [3]. For the amorphous SnO_2 matrix, we take the value $\epsilon_r = 12$ [39,40].

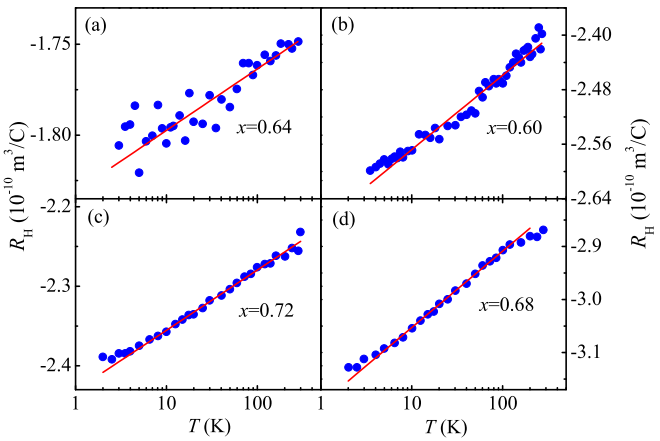

FIG. 2. (Color online) Hall coefficient R_H versus logarithm of temperature for $Ag_x(SnO_2)_{1-x}$ films with x values as indicated. (a) and (b) are data for ~500 nm thick films, and (c) and (d) are data for ~9 nm thick films. The solid straight lines are least-squares fits to Eq. (1).

The D value can be calculated by using the free-electron model and taking the electron mean free path to be the grain size a.

The predications of Eq. (1) are least-squares fitted to our $R_H(T)$ data and shown by the solid straight lines in Figs. 2(a) and 2(b). In our fits, n^* and c_d are adjustable parameters, and g_T is independently determined from comparison of the measured $\sigma(T)$ data with the predictions of Eq. (3) (see below). Figures 2(a) and 2(b) indicate a good agreement between the theory and experiment. Our extracted values of the relevant parameters are listed in Table I.

Figures 2(c) and 2(d) show the variation of R_H with logarithm of temperature for two 2D films with x as indicated. Similarly, we observe a $R_H \propto \ln T$ law from ~3 to ~300 K. This $\ln T$ behavior can be well described by the predictions of Eq. (1), as given by the solid straight lines. Our least-squares fitted parameters are listed in Table I. Thus, our results presented in this subsection firmly support the theoretical prediction that the $R_H \propto \ln T$ law holds for granular metals in the strong coupling regime and is independent of array dimensionality.

B. Electron-electron interaction effect on longitudinal conductivity in the $g_T \gg g_T^c$ regime

We consider the EEI effect on the temperature behavior of σ in the strong coupling regime of $g_T \gtrsim 5g_T^c$. Figure 3(a) shows the variation of the normalized conductivity $\sigma/\sigma(300\text{K})$ with logarithm of temperature for three 3D thick films with x as indicated. It is seen that $\sigma/\sigma(300\,\text{K}) \propto \ln T$ in the temperature range ~20–100 K. Upon further decrease of temperature, σ deviates from the $\ln T$ dependence and changes to a distinct $\sqrt{T}$ temperature dependence; see the inset of Fig. 3(a).

Figure 3(b) shows the temperature behavior of $\sigma_\square/\sigma_\square(300\,\text{K})$ for three 2D thin films with x as indicated, where $\sigma_\square$ is the sheet conductivity. A $\ln T$ dependence is seen in the temperature range ~20–100 K. Note that at lower

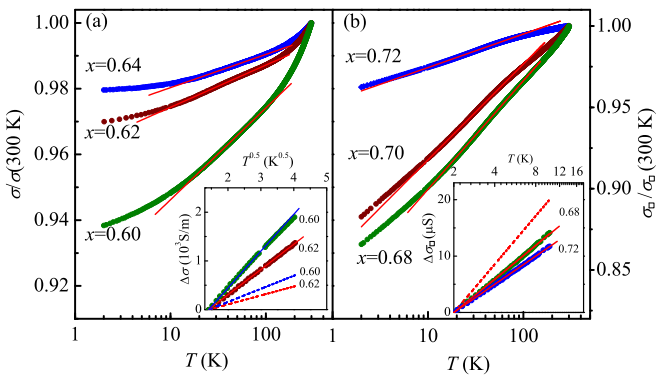

FIG. 3. (Color online) Normalized conductivity $\sigma/\sigma(300\,\text{K})$ versus logarithm of temperature for several (a) ~500 and (b) ~9 nm thick $Ag_x(SnO_2)_{1-x}$ films falling in the strong coupling regime. The solid straight lines are least-squares fits to Eq. (3). Inset (a): Change of conductivity $\triangle\sigma(T)$ versus $\sqrt{T}$ for two ~500 nm thick films. The dashed straight lines are the theoretical predications of Eq. (5a). Inset (b): Change of sheet conductivity $\triangle\sigma_\square(T)$ versus $\log T$ for two ~9 nm thick films. The dashed straight line is the theoretical predication of Eq. (5b). In insets (a) and (b), the solid straight lines are least-squares fits to the Altshuler-Aronov EEI theory, see text.

temperatures ($\lesssim$10 K), $\sigma_\square/\sigma_\square(300\,\text{K})$ shows a different $\ln T$ dependence, with a slope different from that in the higher T region. This demonstrates a crossover of the electronic conduction process from the incoherent tunneling process to the coherent motion process.

According to the recent theory of granular metals [3,12], the electrical-transport processes in the strong coupling regime are dominated by the coherent electron motion on scales larger than the grain size a at $T \lesssim T^*$. At $T^* \lesssim T$ and also $T \lesssim E_c/k_B$, the conductivity is determined by the granular structure and incoherent tunneling processes on the scales of the order of a. Denoting the corrections arising from the incoherent and coherent processes as $\delta\sigma_1$ and $\delta\sigma_2$, respectively, one can write the total conductivity as follows [3,12]:

$$\sigma = \sigma_0 + \delta\sigma_1 + \delta\sigma_2 \tag{2}$$

with

$$\delta\sigma_1 = -\frac{\sigma_0}{2\pi g_T \tilde{d}} \ln\left[\frac{g_T E_c}{\max(k_B T, g_T \tilde{\delta})}\right] \tag{3}$$

and

$$\delta\sigma_2 = \begin{cases} \frac{\alpha\sigma_0}{12\pi^2 g_T}\sqrt{\frac{k_B T}{g_T \tilde{\delta}}}, & \tilde{d} = 3, \\ -\frac{\sigma_0}{4\pi^2 g_T}\ln\left(\frac{g_T\tilde{\delta}}{k_B T}\right), & \tilde{d} = 2, \end{cases} \tag{4}$$

where σ_0 is the classical conductivity without the EEI effect, $\tilde{d}$ is the dimensionality of the granular array, and $\alpha \approx 1.83$ is a numerical constant. Note that the $\delta\sigma_1$ term is a specific consequence of the presence of granularity. On the other hand, the $\delta\sigma_2$ term essentially recovers the well-established Altshuler-Aronov result for homogeneous disordered metals [41]. Because electron screening is seriously degraded in the presence of granularity, by simply setting the screening factor $\tilde{F} = 0$ in the Altshuler-Aronov theory, one obtains Eq. (4) [42].

We first ignore the $\delta\sigma_2$ term and fit the measured $\sigma(T)$ data between ~20 and ~100 K to Eq. (2), by adjusting the two parameters σ_0 and g_T. The solid straight lines in the main panels of Figs. 3(a) and 3(b) show our best fits. The extracted values of σ_0 and g_T are listed in Table I. A good agreement between the theory and experiment is observed. Inspection of Table I indicates a decreasing g_T value with decreasing x. For example, in 3D films, g_T rapidly decreases from 12 to 4.4 as x is reduced from 0.64 to 0.60. In 2D films, g_T decreases from 9.1 to 2.8 as x is reduced from 0.72 to 0.68. It is worth noting that the fitted values of σ_0 listed in Table I are equal to the measured values of $\sigma(100\,\text{K})$ to within ~5%, suggesting quantitative agreement between theory and experiment. Above ~100 K, the influence of the EEI effect on $\sigma(T)$ can be ignored, because the upper bound temperature for Eq. (3) to be valid is $E_c/k_B \approx 200\pm60$ K in our films.

We in turn consider the low temperature regime of $T \lesssim T^*$. In this regime, the effect of the electron coherent motion at distances far exceeding a must be taken into account. The physical meaning for T^* is that at this characteristic crossover temperature the effective thermal diffusion length $L_{\text{eff}} = \sqrt{\hbar D_{\text{eff}}/(k_B T)} = a$, where D_{eff} is the effective electron diffusion constant in the array. For a periodic cubic granular array, one can write $\sigma_0 = (2e^2/\hbar) g_T a^{2-\tilde{d}}$ and $D_{\text{eff}} = g_T \tilde{\delta} a^2/\hbar$.

Thus, by defining $\triangle\sigma = \sigma(T) - \sigma(T_0)$ for 3D and $\triangle\sigma_\square = \sigma_\square(T) - \sigma_\square(T_0)$ for 2D, and T_0 is a reference temperature (taken to be 2 K in this work), Eq. (4) can be rewritten into the forms

$$\triangle\sigma(T) = \frac{\alpha e^2}{6\pi^2\hbar}\sqrt{\frac{k_B}{\hbar D_{\rm eff}}}(\sqrt{T} - \sqrt{T_0}), \quad \tilde{d} = 3, \quad \text{(5a)}$$

$$\triangle\sigma_\square(T) = \frac{e^2}{2\pi^2\hbar}\ln\left(\frac{T}{T_0}\right). \quad \tilde{d} = 2, \quad \text{(5b)}$$

The inset of Fig. 3(c) [3(d)] shows our measured $\triangle\sigma(T)$ [$\triangle\sigma_\square(T)$] as a function of $\sqrt{T}$ ($\log T$) for two 3D (2D) films with x as indicated. The dashed straight lines in the inset of Fig. 3(c) [3(d)] are the theoretical predications of Eq. (5a) [(5b)]. The experimental data deviate from the theoretical curves. One reason for these deviations may be due to ignoring the electron screening in the formulation of Eqs. (5a) and (5b). We can recover the Altshuler-Aronov EEI results by multiplying the factors $(1 - 9\tilde{F}/8)$ and $(1 - 3\tilde{F}/4)$ on the right-hand side of Eqs. (5a) and (5b), respectively, and then compare the expressions with our data. The solid straight lines in the inset of Fig. 3(a) [3(b)] are the least-squares fits. In 2D films, our fitted values of the screening factor $\tilde{F}$ are 0.56 and 0.41 for the $x = 0.72$ and 0.68 films, respectively. In 3D films, the values are -1.63 and -1.61 for the $x = 0.62$ and 0.60 films, respectively. Since $\tilde{F}$ should lie between 0 and 1 in the Altshuler-Aronov theory, the seemingly good fits shown in the inset of Fig. 3(a) are thus spurious. This issue requires further theoretical clarification.

C. Logarithmic temperature behavior of electronic transport near the percolation threshold

1. *Logarithmic temperature dependence of longitudinal conductivity*

In terms of the EEI effect, the major difference between a granular metal and a homogeneous disordered metal is that the presence of granularity in the former seriously restrains the screening of electrons. As a consequence, the Coulomb interaction is markedly enhanced [43,44]. Since the electron screening is sustained by intergrain tunneling, the degree of screening naturally degrades with decreasing g_T [3]. It is thus meaningful to examine the temperature behaviors of σ and R_H as g_T is reduced from the strong coupling regime (taken to be $g_T \gtrsim 5g_T^c$ in this work, as mentioned) to the critical regime near the percolation threshold ($g_T \to g_T^c$).

Figures 4(a) [4(b)] shows the variation of the normalized conductivity $\sigma/\sigma(300\,\text{K})$ with logarithm of temperature for three 3D (2D) films with x values slightly higher than x_c. It is seen that the $\sigma/\sigma(300\,\text{K}) \propto \ln T$ law holds in a wide T range ~20–100 K in both 3D and 2D films. For films lying in the strong coupling regime, the relative change in $\sigma/\sigma(300\,\text{K})$ is small [~ a few percent, Figs. 3(a) and 3(b)]. On the other hand, for films lying near the percolation threshold, the relative conductivity change is considerably larger (~ tens of percent). As an experimental fact, the $\ln T$ dependence of σ as $x \to x_c$ in different granular metals has been reported by several groups in past decades [24–33]. Yet the physical origin has not been fully understood. Since the strength of the EEI effect progressively

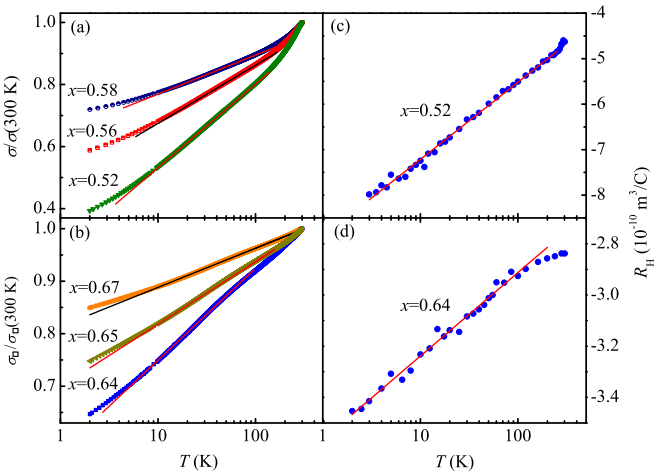

FIG. 4. (Color online) Normalized conductivity $\sigma/\sigma(300\,\text{K})$ versus logarithm of temperature for (a) ~500 and (b) ~9 nm thick $Ag_x(SnO_2)_{1-x}$ films near the percolation threshold. The solid straight lines are least-squares fits to Eq. (3). Hall coefficient versus logarithm of temperature for (c) ~500 and (d) ~9 nm thick $Ag_x(SnO_2)_{1-x}$ films with $x \to x_c$. The solid straight lines are least-squares fits to Eq. (1).

enhances with decreasing g_T as discussed, we suggest that the robust $\sigma \propto \ln T$ behavior in a wide T range as $g_T \to g_T^c$ originates from the same physics of the EEI effect described in Eq. (3). We elaborate our reasoning below.

Assume that Eq. (3) still holds as the g_T value decreases from the strong coupling $g_T \gg g_T^c$ to the critical regime $g_T \to g_T^c$. We compare our experimental $\sigma(T)$ data with this equation. The solid straight lines in Figs 4(a) and 4(b) are the least-squares fits to Eq. (2) (the $\delta\sigma_2$ term is ignored by focusing on the data at $T \gtrsim 20$ K). The fitted values of σ_0 and g_T are listed in Table I. Inspection of Table I indicates that our extracted σ_0 and g_T values monotonically and smoothly decrease with decreasing x from the strong coupling regime to near the percolation threshold. This result strongly suggests that Eq. (3) is qualitatively valid down to $x \to x_c$.

We may further extract the g_T^c values in our films and compare with the theoretical estimates. In 3D films near x_c, our fitted g_T values are $g_T(x = 0.56) \simeq 0.58$ and $g_T(x = 0.52) \simeq 0.34$. By a linear extrapolation, we extract the value $g_T^{c,3D}(x_c^{3D} \simeq 0.50) \simeq 0.22$. Similarly, in 2D films, we obtain $g_T^{c,2D}(x_c^{2D} \simeq 0.63) \simeq 0.5$. The theoretical expression of g_T^c for $\tilde{d}$ array dimensionality is $g_T^c = (1/2\pi\tilde{d})\ln(E_c/\tilde{\delta})$ [3]. By substituting the values of $\tilde{d}$, E_c, and $\tilde{\delta}$ (Ref. [45]), we obtain $(g_T^{c,3D})_{\rm th} \simeq 0.21$ and $(g_T^{c,2D})_{\rm th} \simeq 0.32$. Thus, the experimental and theoretical g_T^c values are in good agreement. This self-consistency check provides a strong support for our proposition that the same EEI effect is responsible for the $\sigma \propto \ln T$ behavior repeatedly observed in granular metals as $x \to x_c$ [24–33].

2. *Logarithmic temperature dependence of Hall coefficient*

Figures 4(c) and 4(d) respectively show the variation of R_H with logarithm of temperature for one 3D and one 2D films with x close to x_c. It is clearly seen that the $R_H \propto \ln T$ law holds from ~3 (2) K to ~230 (160) K in the 3D (2D) film.

Again, we propose to attribute this robust $\ln T$ behavior to the EEI effect in granular metals. Our reasoning is as follows.

Assume that Eq. (1) still holds as $x \to x_c$. We compare the experimental $R_H(T)$ data with the predication of this equation. Our least-squares fits (the solid straight lines) are shown in Figs. 4(c) and 4(d), and the extracted values of the adjustable parameters c_d and n^* are listed in Table I. The fact that our fitted c_d and n^* values are acceptable suggests that Eq. (1) is qualitatively valid near the percolation threshold [46]. Furthermore, the upper bound temperature for the $\ln T$ law to hold is given by $T^H_{\max} = \min(g_T E_c, E_{Th})/k_B$. By taking $T^H_{\max} \approx E_c/k_B$, we obtain a dimensionality independent theoretical estimate $(T^H_{\max})_{\rm th} \approx 200$ K. This estimate is in good agreement with our experimental values given above. This result provides a further support for the qualitative validity of Eq. (1) as $x \to x_c$. Note that in Figs. 4(c) and 4(d), R_H changes by a few tens of percent in the $\ln T$ temperature range, which are much bigger than those revealed in Fig. 2.

IV. CONCLUSION

We have studied the Hall coefficient R_H and longitudinal conductivity σ in 3D and 2D Ag-SnO_2 granular films. Our films span from the strong coupling regime to the regime near the percolation threshold. In the $g_T \gg g_T^c$ strong tunneling regime, we observed a $R_H \propto \ln T$ law as well as a $\sigma \propto \ln T$ law in a wide temperature range. These logarithmic temperature dependences, which are independent of array dimensionality, are successfully ascribed to the EEI effect in the presence of granularity. At lower temperatures, as the effective thermal diffusion length becomes longer than the grain size, a crossover of σ to the EEI effect characteristic of homogeneous disordered metals was observed. Furthermore, we found that the EEI-effect-induced corrections to R_H and σ as predicted by the recent theory of granular metals can be extended to the regime near the percolation threshold. We propose an explanation for the long-standing puzzle of the logarithmic temperature dependence of conductivity which has previously been frequently observed in composite systems as $x \to x_c$.

ACKNOWLEDGMENTS

The authors thank Y. J. Zhang for her careful reading of the manuscript. This work was supported by the National Natural Science Foundation of China (NSFC) through Grant No. 11174216 and the Research Fund for the Doctoral Program of Higher Education through Grant No. 20120032110065 (Z.Q.L.), and by the Taiwan Ministry of Science and Technology (MOST) through Grant No. NSC 103-2112-M-009-017-MY3 and the MOE ATU Program (J.J.L.).

[1] B. Abeles, P. Sheng, M. D. Coutts, and Y. Arie, Adv. Phys. **24**, 407 (1975).
[2] B. Abeles, *Applied Solid State Science: Advance in Materials and Device Research*, edited by R. Wolf (Academic, New York, 1976).
[3] I. S. Beloborodov, A. V. Lopatin, V. M. Vinokur, and K. B. Efetov, Rev. Mod. Phys. **79**, 469 (2007).
[4] M. Yu. Kharitonov and K. B. Efetov, Phys. Rev. Lett. **99**, 056803 (2007).
[5] A. Gerber, A. Milner, G. Deutscher, M. Karpovsky, and A. Gladkikh, Phys. Rev. Lett. **78**, 4277 (1997).
[6] X. X. Zhang, C. Wan, H. Liu, Z. Q. Li, P. Sheng, and J. J. Lin, Phys. Rev. Lett. **86**, 5562 (2001).
[7] C. Wan and P. Sheng, Phys. Rev. B **66**, 075309 (2002).
[8] Y. N. Wu, Z. Q. Li, and J. J. Lin, Phys. Rev. B **82**, 092202 (2010).
[9] P. Sheng, E. K. Sichel, and J. I. Gittleman, Phys. Rev. Lett. **40**, 1197 (1978).
[10] G. Ambrosetti, I. Balberg, and C. Grimaldi, Phys. Rev. B **82**, 134201 (2010).
[11] C. Grimaldi, Phys. Rev. B **89**, 214201 (2014).
[12] I. S. Beloborodov, K. B. Efetov, A. V. Lopatin, and V. M. Vinokur, Phys. Rev. Lett. **91**, 246801 (2003).
[13] K. B. Efetov and A. Tschersich, Phys. Rev. B **67**, 174205 (2003).
[14] K. B. Efetov and A. Tschersich, Europhys. Lett. **59**, 114 (2002).
[15] M. Yu. Kharitonov and K. B. Efetov, Phys. Rev. B **77**, 045116 (2008).
[16] L. Rotkina, S. Oh, J. N. Eckstein, and S. V. Rotkin, Phys. Rev. B **72**, 233407 (2005).
[17] R. Sachser, F. Porrati, C. H. Schwalb, and M. Huth, Phys. Rev. Lett. **107**, 206803 (2011).
[18] P. Achatz, W. Gajewski, E. Bustarret, C. Marcenat, R. Piquerel, C. Chapelier, T. Dubouchet, O. A. Williams, K. Haenen, J. A. Garrido, and M. Stutzmann, Phys. Rev. B **79**, 201203(R) (2009).
[19] Y. C. Sun, S. S. Yeh, and J. J. Lin, Phys. Rev. B **82**, 054203 (2010).
[20] Y. J. Zhang, Z. Q. Li, and J. J. Lin, Phys. Rev. B **84**, 052202 (2011).
[21] Analytical results can also be obtained for the opposite limit of $g_T \ll 1$ (Refs. [3, 13]). In this work we focus on the metallic side of the metal-insulator transition.
[22] C. Kittel, *Introduction to Solid State Physics*, 8th ed. (Wiley, New York, 2005).
[23] Y. F. Wei and Z. Q. Li, Appl. Phys. Lett. **102**, 131911 (2013).
[24] N. Savvides, S. P. McAlister, C. M. Hurd, and I. Shiozaki, Solid State Commun. **42**, 143 (1982).
[25] R. W. Simon, B. J. Dalrymple, D. Van Vechten, W. W. Fuller, and S. A. Wolf, Phys. Rev. B **36**, 1962 (1987).
[26] A. B. Pakhomov, X. Yan, and B. Zhao, Appl. Phys. Lett. **67**, 3497 (1995).
[27] X. N. Jing, N. Wang, A. B. Pakhomov, K. K. Fung, and X. Yan, Phys. Rev. B **53**, 14032 (1996).
[28] A. B. Pakhomov and X. Yan, Solid State Commun. **99**, 139 (1996).
[29] B. Zhao and X. Yan, J. Appl. Phys. **81**, 4290 (1997).
[30] Q. Y. Xu, G. Ni, M. H. Pan, H. Sang, and Y. W. Du, J. Phys.: Condens. Matter. **13**, 1851 (2001).
[31] D. L. Peng, T. Hihara, and K. Sumiyama, Phys. Status Solidi A **196**, 450 (2003).
[32] H. Liu, R. K. Zheng, G. H. Wen, and X. X. Zhang, Vacuum **73**, 603 (2004).

[33] J. C. Denardin, M. Knobel, L. S. Dorneles, and L. F. Schelp, J. Magn. Magn. Mater. **294**, 206 (2005).
[34] B. L. Altshuler, D. Khmel'nitzkii, A. I. Larkin, and P. A. Lee, Phys. Rev. B **22**, 5142 (1980).
[35] P. A. Lee and T. V. Ramakrishnan, Rev. Mod. Phys. **57**, 287 (1985).
[36] G. Bergmann, Phys. Rep. **107**, 1 (1984).
[37] G. Bergmann, Int. J. Mod. Phys. B **24**, 2015 (2010).
[38] J. J. Lin and J. P. Bird, J. Phys.: Condens. Matter **14**, R501 (2002).
[39] D. Jousse, Phys. Rev. B **31**, 5335 (1985).
[40] M. Kojima, H. Kato, A. Imai, and A. Yoshida, J. Appl. Phys. **64**, 1902 (1988).
[41] B. L. Altshuler and A. G. Aronov, in *Electron-Electron Interactions in Disordered Systems*, edited by A. L. Efros and M. Pollak (Elsevier, Amsterdam, 1985).
[42] See, for example, C. Y. Wu, W. B. Jian, and J. J. Lin, Phys. Rev. B **52**, 15479 (1995), for discussion of the screening factor $\tilde{F}$ (F) in the Altshuler-Aronov theory.
[43] S. Chakravarty, S. Kivelson, and G. T. Zimanyi, B. I. Halperin, Phys. Rev. B **35**, 7256(R) (1987).
[44] I. S. Beloborodov, K. B. Efetov, A. Altland, and F. W. J. Hekking, Phys. Rev. B **63**, 115109 (2001).
[45] For our pure Ag film, the measured carrier concentration is $n \simeq 8.1 \times 10^{28}$ m^{-3}. Using the free-electron model, we obtain a density of states $N(E_F) \simeq 1.1 \times 10^{47}$ states/(J m^3), which is within $\sim$10% of the textbook value (Ref. [22]). The mean energy level spacing for a grain size $a \approx 7$ nm is then $\tilde{\delta} \approx 5.0 \times 10^{-23}$ J.
[46] The n^* value extracted for the $x \simeq 0.52$ films is a factor of $\sim$ 2–3 lower than those in other films. This low value is likely owing to $x \to x_c$.